Optimality of the fully discrete filtered backprojection algorithm for tomographic inversion

Andreas Rieder · Arne Schneck

Abstract Although the filtered backprojection algorithm (FBA) has been the standard reconstruction algorithm in 2D computerized tomography for more than 30 years, its convergence behavior is not completely settled so far. Relying on convergence results by Rieder and Faridani for the semi-discrete FBA [SIAM J. Numer. Anal., 41(3), 869–892, 2003], we show optimality of the fully discrete version for reconstructing sufficiently smooth density distributions. Further, we introduce MFBA, a modified version of FBA, and prove its optimality under weaker smoothness requirements. Remarkably MFBA may have a larger convergence order in the angular than in the lateral variable, thus allowing optimal convergence in case of angular undersampling. Moreover, MFBA can be seen as a limit of the phantom view method introduced to increase angular resolution.

Mathematics Subject Classifications (2000) 65R20

1 Introduction

X-Ray computerized tomography (CT) is a technique for imaging the density distribution inside an object. Mathematically speaking, CT reduces to reconstructing a function from its integrals along straight lines, see, e.g., Natterer [11] for details.

A. Rieder (✉)
Institut für Angewandte und Numerische Mathematik and Institut für Wissenschaftliches Rechnen
und Mathematische Modellbildung, Universität Karlsruhe, 76128 Karlsruhe, Germany
e-mail: andreas.rieder@math.uni-karlsruhe.de
URL: http://www.mathematik.uni-karlsruhe.de/ianm3/~rieder

A. Schneck
Graduiertenkolleg 1294 "Analysis, Simulation and Design of Nanotechnological Processes",
Fakultät für Mathematik, Universität Karlsruhe, 76128 Karlsruhe, Germany
e-mail: arne.schneck@math.uni-karlsruhe.de

🄐 Springer

The mathematical model in 2D is the *Radon transform*

$$\mathbf{R} f(s, \vartheta) := \int_{L(s,\vartheta)} f(x) \, d\sigma(x),$$

mapping a function to its integrals over the lines $L(s, \vartheta) = \{\tau \, \omega^{\perp}(\vartheta) + s \, \omega(\vartheta) \mid \tau \in \mathbb{R}\}$ where $s \in \mathbb{R}$, $\omega(\vartheta) = (\cos \vartheta, \sin \vartheta)^t$, and $\omega^{\perp}(\vartheta) = (-\sin \vartheta, \cos \vartheta)^t$ for $\vartheta \in [0, \pi]$. We assume throughout that the searched-for density distributions are compactly supported in Ω, the unit disk in $\mathbb{R}^2$ centered about the origin. Thus, the lateral variable s may be restricted to $[-1, 1]$.

In the *parallel scanning geometry* we observe the discrete Radon data

$$D = \{\mathbf{R} f(kh, jh_\vartheta) : k = -q, \ldots, q, \ j = 0, \ldots, p - 1\}, \quad p, q \in \mathbb{N}, \quad (1.1)$$

where $h = 1/q$ is the lateral sampling rate and $h_\vartheta = \pi/p$ is the angular sampling rate. Let $f_{\text{FBA}} = f_{\text{FBA}}(h, h_\vartheta)$ denote the reconstruction of f by the filtered backprojection algorithm (FBA) from D. Then, we will show that[1]

$$\|f - f_{\text{FBA}}\|_{L^2(\Omega)}$$
$$\lesssim \left(h^{\min\{\alpha_{\max}, \alpha\}} + h_\vartheta^\alpha + h_\vartheta h^{\min\{\alpha_{\max}, \alpha-1\}} \right) \|f\|_{H_0^\alpha(\Omega)}, \quad \alpha \geq 1. \quad (1.2)$$

The maximal lateral convergence rate $\alpha_{\max}$ depends on the used filter and the interpolation process after filtering. For instance,

$$\alpha_{\max} = \begin{cases} 3/2 & \text{Shepp-Logan filter with piecewise constant interpolation,} \\ 2 & \text{Shepp-Logan filter with piecewise linear interpolation,} \\ 5/2 & \text{mod. Shepp-Logan filter with piecewise linear interpolation.} \end{cases} \quad (1.3)$$

In principle, it is possible to construct filters and adapted local interpolation schemes leading to arbitrarily large $\alpha_{\max}$ (see Remark 3.2).

Under the optimal sampling condition $p = \pi q$ ($h = h_\vartheta$), see, e.g., Natterer [11, Table III.1], our estimate (1.2) yields the convergence rate h^α as $h \to 0$ which is optimal for density distributions in $H_0^\alpha(\Omega)$, see Natterer [10] or [11, Theorem IV.2.2].

Moreover, we introduce algorithm MFBA, a modification of FBA, and we prove that

$$\|f - f_{\text{MFBA}}\|_{L^2(\Omega)}$$
$$\lesssim \left(h^{\min\{\alpha_{\max}, \alpha\}} + h_\vartheta^{\min\{5/2 - \epsilon, \alpha\}} \right) \|f\|_{H_0^\alpha(\Omega)}, \quad \alpha > 1/2, \quad (1.4)$$

for any $\epsilon > 0$ where $\alpha_{\max}$ is as in (1.3). So we can ensure optimality of MFBA for a larger range of Sobolev orders compared to FBA. Note also that the convergence

---

[1] $A \lesssim B$ indicates the existence of a generic constant c such that $A \leq cB$ uniformly in all parameters A and B may depend on.

order in h_ϑ may exceed the order in h. Accordingly optimal convergence in the lateral variable can be achieved while under-sampling the angular variable (in case $\alpha_{\max} < 5/2$ and α large enough). Further, we relate MFBA to the streak-alleviating phantom view method. Phantom views are created by interpolating the Radon data linearly with respect to the angular variable, see Lewitt et al. [6] and Weiss et al. [17]. Since the phantom view method converges to MFBA as the number of phantom views increases, its convergence behavior essentially coincides with (1.4).

The paper is organized as follows. In the next section we introduce the filtered backprojection algorithm, recall the convergence result of Rieder and Faridani [12], and give some stability estimates for the Radon transform which we will need later. Then we present and prove our convergence estimate for the fully discrete FBA in Sect. 3. Section 4 is devoted to our modified filtered backprojection algorithm: We motivate its definition, prove convergence, and discuss some aspects of its implementation. Further, the phantom view method is introduced and its relation to MFBA is established. Numerical experiments visualize our convergence results in the final section where also qualitative comparisons of the algorithms are presented.

2 The filtered backprojection algorithm

In this section we introduce the FBA in detail and recall results which we will need later.

First, we present some notation. Let $\widehat{f}(\xi) := (2\pi)^{-d/2} \int_{\mathbb{R}^d} f(x) e^{-\iota \xi^t x} \, dx$ denote the Fourier transform of a function f in $L^1(\mathbb{R}^d) \cap L^2(\mathbb{R}^d)$. The Fourier transform can be extended to L^2-functions and tempered distributions by continuity and duality. We define the Sobolev spaces $H^\alpha(\mathbb{R}^d)$, $\alpha \in \mathbb{R}$, to be the closure of the Schwartz class with respect to the norm

$$\|f\|_\alpha^2 := \int_{\mathbb{R}^d} (1 + |\xi|^2)^\alpha \, |\widehat{f}(\xi)|^2 \, d\xi.$$

Starting point for deriving the FBA is the inversion formula

$$f = \frac{1}{4\pi} \mathbf{R}^*(\Lambda \otimes I) \mathbf{R} f$$

which holds true for $f \in L^2(\Omega)$ [12, Sect. 3.2][2]. Here, the *backprojection operator*

$$\mathbf{R}^* g(x) = \int_0^{2\pi} g(x^t \omega(\vartheta), \vartheta) \, d\vartheta \tag{2.1}$$

---

[2] Later in the paper we will benefit from the 2π-periodicity of $\mathbf{R} f(s, \cdot)$. Therefore, the angular variable from now on runs in the interval $[0, 2\pi]$. From a practical point of view, however, it suffices to know $\mathbf{R} f$ on $[-1, 1] \times [0, \pi]$ to recover f.

is the adjoint of $\mathbf{R} \in \mathcal{L}\left(L^2(\Omega), L^2(Z)\right)$ with $Z = [-1, 1] \times [0, 2\pi]$. The Λ-operator is defined by

$$\widehat{\Lambda u}(\xi) = |\xi| \widehat{u}(\xi)$$

and maps $H^\alpha(\mathbb{R}^d)$ boundedly to $H^{\alpha-1}(\mathbb{R}^d)$. The binary operation $\otimes$ denotes the tensor product of operators and spaces, respectively, see, e.g., Aubin [1]. Therefore, Λ in $(\Lambda \otimes I)\mathbf{R}f$ only affects the lateral variable (I is the identity).

Due to Rieder and Faridani [12] FBA can be written as

$$f_{\text{FBA}}(x) := \mathbf{R}^*_{h_\vartheta} (\mathrm{I}_h \Lambda E_h \otimes I)\mathbf{R}f(x) \tag{2.2}$$

where

$$\mathbf{R}^*_{h_\vartheta} g(x) := h_\vartheta \sum_{j=0}^{2p-1} g(x^t \omega(\vartheta_j), \vartheta_j), \quad \vartheta_j = j h_\vartheta.$$

The operators E_h and I_h are generalized interpolation operators: For $u \in H^\alpha(\mathbb{R})$ define

$$E_h u(s) := h^{-1} \sum_{k \in \mathbb{Z}} \langle u, \epsilon_h(\cdot - s_k)\rangle \ B_h(s - s_k) \tag{2.3}$$

where $\epsilon_h(s) = \epsilon(s/h)$ and $B_h(s) = B(s/h)$. Here, $B \in L^2(\mathbb{R})$ is the "interpolation function" and $\epsilon \in H^{-\alpha}(\mathbb{R})$ is assumed to be even with $\widehat{\epsilon}(0) = 1/\sqrt{2\pi}$. Further, $\langle \cdot, \cdot \rangle$ denotes the duality pairing in $H^\alpha(\mathbb{R}) \times H^{-\alpha}(\mathbb{R})$. For $u \in H^\alpha(\mathbb{R})$, $\alpha > 1/2$, we may choose $\epsilon = \delta$ (Dirac distribution). In this case, $h^{-1}\langle u, \epsilon_h(\cdot - s_k)\rangle = u(s_k)$. Other choices of ϵ allow to model finite width of the rays and detector inhomogeneities. Indeed, for ϵ being a non-negative function compactly supported in $[-1/2, 1/2]$ with a normalized mean value we observe the discrete Radon data

$$\{g_{k,j} : k = -q, \ldots, q, \ j = 0, \ldots, p - 1\}$$

where

$$g_{k,j} = h^{-1} \left\langle \mathbf{R}f(\cdot, \vartheta_j), \epsilon_h(\cdot - s_k)\right\rangle = h^{-1} \int\limits_{s_k - h/2}^{s_k + h/2} \mathbf{R}f(s, \vartheta_j)\, \epsilon_h(s - s_k)\, \mathrm{d}s.$$

Therefore ϵ can be interpreted as *sensitivity profile* of the X-ray detectors.

Analogously, we define

$$\mathrm{I}_h u(s) := h^{-1} \sum_{k \in \mathbb{Z}} \langle u, \eta_h(\cdot - s_k)\rangle \ A_h(s - s_k), \tag{2.4}$$

where η and A play the roles of ϵ and B, respectively. For more details on E_h and I_h we refer to [12, Sect. 3.2].

Some straightforward calculations reveal that

$$(I_h \Lambda E_h \otimes I)\mathbf{R}f(s, \vartheta) = \sum_{\ell \in \mathbb{Z}} \left(\sum_{k \in \mathbb{Z}} w_{\ell-k} \langle \mathbf{R}f(\cdot, \vartheta), \epsilon_h(\cdot - s_k) \rangle \right) A_h(s - s_\ell) \quad (2.5)$$

with $w_r = \upsilon(r)/h^2$ where

$$\upsilon(s) := \frac{1}{\pi} \int_0^\infty \sigma \, \widehat{B}(\sigma) \, \widehat{\eta}(\sigma) \cos(s\sigma) \mathrm{d}\sigma$$

is the *reconstruction filter*. Thus, the evaluation of $f_{\mathrm{FBA}}(x)$ can be implemented exactly as in [11, Chap. V.1.1]. The sum over k in (2.5) represents the filtering step.

We require the following approximation properties of E_h and I_h, respectively:

(i)   There are non-negative constants $\tau_{\max}$ and $\beta_{\min} \le \beta_{\max}$ such that

$$\|E_h u - u\|_\tau \lesssim h^{\beta-\tau} \|u\|_\beta \quad (2.6)$$

for $\beta_{\min} \le \beta \le \beta_{\max}$, $1/2 \le \tau \le \tau_{\max}$, $\tau \le \beta$ and any $u \in H_0^\beta(-1, 1)^3$.
(ii) There is a constant $\alpha_I > 0$ such that

$$\|I_h - I\|_{H^{\alpha-1/2}(\mathbb{R}) \to H^{-1/2}(\mathbb{R})} \lesssim h^\alpha \quad (2.7)$$

for $0 \le \alpha \le \alpha_I$.

Both estimates, (2.6) and (2.7), are meant asymptotically as $h \to 0$. All further estimates involving h or h_ϑ have to be understood in similar manner.

Rieder and Faridani studied a semi-discrete version of FBA, that is, they did not consider discretization of the angular variable. Their result [12, Theorem 3.7] is formulated in the following theorem (Natterer [9] gave a convergence result for the other semi-discrete version of FBA where the angular variable is discretized but not the lateral).

Theorem 2.1 *Under* (2.6) *and* (2.7) *with* $\beta_{\max}, \tau_{\max} \ge 1/2$ *we have that*

$$\left\| f - \frac{1}{4\pi} \mathbf{R}^*(I_h \Lambda E_h \otimes I)\mathbf{R}f \right\|_{L^2(\Omega)} \lesssim h^\alpha \|f\|_\alpha$$

for $\max\{0, \beta_{\min} - 1/2\} \le \alpha \le \min\{\alpha_I, \beta_{\max} - 1/2, \tau_{\max} - 1/2\}$ *and* $f \in H_0^\alpha(\Omega)$.

---

3 $H_0^\alpha(D)$ is the closure of $\mathcal{C}_0^\infty(D)$, the space of infinitely differentiable functions compactly supported in $D \subset \mathbb{R}^d$, with respect to the norm $\| \cdot \|_\alpha$.

We present concrete examples; for proofs see again [12]. Set

$$\widetilde{f}_{\text{FBA}} = \frac{1}{4\pi} \mathbf{R}^*(I_h \Lambda E_h \otimes I) \mathbf{R} f.$$

Example 2.2 (Shepp-Logan filter with nearest-neighbor interpolation) Let $B(\cdot) = \text{sinc}(\pi \cdot)^4$ be the interpolating function in E_h and $A = \mathbf{1}_{[-1/2,1/2]}[5]$ the interpolating function in I_h. Further, let $\eta = \mathbf{1}_{[-1/2,1/2]}$ in I_h. Then, the discrete filter $\{w_r\}_{r\in\mathbb{Z}}$ in (2.5) is the Shepp-Logan filter [15]:

$$w_r = \frac{2}{\pi^2 h^2} \frac{1}{1 - 4r^2}. \tag{2.8}$$

Further,

$$\left\| \widetilde{f}_{\text{FBA}} - f \right\|_{L^2(\Omega)} \lesssim h^{\min\{3/2, \alpha\}} \|f\|_\alpha \quad \text{for } f \in H_0^\alpha(\Omega), \ \alpha > 0,$$

as long as ϵ in E_h is either an even, compactly supported and normalized L^2-function or the Dirac distribution.

Example 2.3 (Shepp-Logan filter with piecewise linear interpolation) Let E_h and I_h be as in Example 2.2, except for A which is now the linear B-spline, that is, $A = \mathbf{1}_{[-1/2,1/2]} \star \mathbf{1}_{[-1/2,1/2]}$. Hence, I_h interpolates piecewise linear. The discrete filter $\{w_r\}_{r\in\mathbb{Z}}$ is as in (2.8). Here, we have

$$\left\| \widetilde{f}_{\text{FBA}} - f \right\|_{L^2(\Omega)} \lesssim h^{\min\{2, \alpha\}} \|f\|_\alpha \quad \text{for } f \in H_0^\alpha(\Omega), \ \alpha > 0.$$

Example 2.4 (modified Shepp-Logan filter with piecewise linear interpolation) Let E_h and I_h be as in Example 2.3, except for η which is now given by

$$\widehat{\eta}(\sigma) = (2\pi)^{-1/2} \frac{\text{sinc}(\sigma/2)}{3/4 + \cos(\sigma)/4}.$$

The corresponding discrete filter $\{w_r\}_{r\in\mathbb{Z}}$ is called modified Shepp-Logan filter [12]. Here,

$$\left\| \widetilde{f}_{\text{FBA}} - f \right\|_{L^2(\Omega)} \lesssim h^{\min\{5/2, \alpha\}} \|f\|_\alpha \quad \text{for } f \in H_0^\alpha(\Omega), \ \alpha > 0.$$

For later use we compile Sobolev space estimates of the Radon transform. Set $H^{(\alpha,\beta)} := H^\alpha(\mathbb{R}) \otimes H_p^\beta(0, 2\pi)[6]$. Due to Natterer and Louis [8] we have

$$\|\mathbf{R}f\|_{H^{(\alpha+1/2,0)}} \lesssim \|f\|_\alpha \quad \text{for any } f \in H_0^\alpha(\Omega), \ \alpha \geq 0.$$

A similar continuity estimate by Rieder and Schuster [13] yields especially

$$\|\mathbf{R}f\|_{H^{(0,\alpha+1/2)}} \lesssim \|f\|_\alpha \quad \text{for any } f \in H_0^\alpha(\Omega), \ \alpha \geq 0.$$

---

[4] sinc is the *sinus cardinalis*: $\text{sinc}(s) = (\sin s)/s$.

[5] $\mathbf{1}_D$ denotes the indicator function of D.

[6] For the definition of the Sobolev spaces $H_p^\beta(a, b)$ of periodic functions with period $b-a$, see, for instance, Lions and Magenes [7, Chap. 1.7].

Interpolating both latter mapping properties of **R** finally results in

$$\|\mathbf{R}f\|_{H^{(\beta,\alpha+1/2-\beta)}} \lesssim \|f\|_\alpha \quad \text{for any } 0 \le \beta \le \alpha + 1/2 - \beta \tag{2.9}$$

and $f \in H_0^\alpha(\Omega)$.

3 Convergence of the fully discrete FBA

In this section we will prove our asymptotic convergence estimate of FBA which is stated in the following theorem.

Theorem 3.1 *Under* (2.6) *and* (2.7) *with* $\beta_{\max}, \tau_{\max} \ge 3/2$ *we have that*

$$\left\| f - \frac{1}{4\pi}\mathbf{R}^*_{h_\vartheta}(\mathrm{I}_h \Lambda E_h \otimes I)\mathbf{R}f \right\|_{L^2(\Omega)}$$
$$\lesssim \left(h^{\min\{\alpha_{\max},\alpha\}} + h_\vartheta^\alpha + h_\vartheta h^{\min\{\alpha_{\max},\alpha-1\}} \right) \|f\|_\alpha, \quad \alpha \ge \alpha_{\min},$$

where $\alpha_{\min} = \max\{1, \beta_{\min} - 1/2\}$, $\alpha_{\max} = \min\{\alpha_{\mathrm{I}}, \beta_{\max} - 1/2, \tau_{\max} - 1/2\}$, *and* $f \in H_0^\alpha(\Omega)$.

Note that Theorem 3.1 reduces to (1.2) with $\alpha_{\max}$ from (1.3) for our concrete settings of Examples 2.2, 2.3, and 2.4.

Remark 3.2 In [12, Remark 4.2] Rieder and Faridani sketched a scheme to construct interpolation operators I_h (2.4) with arbitrarily large α_{I}. Further, these interpolation operators are still local since A is a B-spline. Using band-limited interpolation for E_h, that is, $B(\cdot) = \mathrm{sinc}(\pi \cdot)$ and ϵ is the Dirac distribution in (2.3), we have $\beta_{\max} = \tau_{\max} = \infty$, see [12, Theorem B.4]. Thus, one can construct efficient filtered backprojection schemes with an arbitrarily large $\alpha_{\max}$. Of course, one would fully benefit from these highly accurate filtered backprojection schemes if the searched-for density distributions are sufficiently smooth which is not the case in medical imaging but in optical homodyne tomography, see, e.g., Smithey et al. [16]. In optical homodyne tomography one determines the Wigner function of the state of a quantum system.

In the remainder of this section we verify Theorem 3.1. In view of Theorem 2.1 we start with

$$\|f - f_{\mathrm{FBA}}\|_{L^2(\Omega)} \le \left\| f - \frac{1}{4\pi}\mathbf{R}^*(\mathrm{I}_h \Lambda E_h \otimes I)\mathbf{R}f \right\|_{L^2(\Omega)}$$
$$+ \left\| (\mathbf{R}^* - \mathbf{R}^*_{h_\vartheta})(\mathrm{I}_h \Lambda E_h \otimes I)\mathbf{R}f \right\|_{L^2(\Omega)} \tag{3.1}$$

and it remains to investigate the second error term which involves the discretization of the backprojection operator. We once again apply the triangle inequality and obtain

$$
\begin{aligned}
\big\| (\mathbf{R}^* - \mathbf{R}^*_{h_\vartheta}) & (I_h \Lambda E_h \otimes I) \mathbf{R} f \big\|_{L^2(\Omega)} \\
& \leq \big\| (\mathbf{R}^* - \mathbf{R}^*_{h_\vartheta}) \left((I_h \Lambda E_h - \Lambda) \otimes I \right) \mathbf{R} f \big\|_{L^2(\Omega)} \\
& \quad + \big\| (\mathbf{R}^* - \mathbf{R}^*_{h_\vartheta}) (\Lambda \otimes I) \mathbf{R} f \big\|_{L^2(\Omega)} .
\end{aligned}
\tag{3.2}
$$

Following we bound each of the norms on the right hand side.

As $\mathbf{R}^*_{h_\vartheta}$ arises from $\mathbf{R}^*$ by applying the composite trapezoidal rule to the integral in (2.1) we will rely on the following estimate for the quadrature error.

Lemma 3.3 *Let $u \in H_p^{2k+1}(a, b)$ for one $k \in \mathbb{N}_0$. Then,*

$$
\left| \int_a^b u(t)\mathrm{d}t - h \sum_{j=0}^{n-1} u(a + jh) \right| \lesssim h^{2k+1} \int_a^b |u^{(2k+1)}(t)|\mathrm{d}t
$$

where $h = (b - a)/n$ and $n \in \mathbb{N}$.

Proof Since $\big\{ g|_{[a,b]} : g \in \mathcal{C}^{2k+1}(\mathbb{R}),\ g \text{ is } (b - a)\text{-periodic} \big\}$ is dense in $H_p^{2k+1}(a, b)$ the assertion follows for $k \in \mathbb{N}$ readily from the Euler–Maclaurin formula [5, Corollary 9.27] and the bounded embedding $H_p^{2k+1}(a, b) \hookrightarrow \mathcal{C}([a, b])$. For $k = 0$ the statement may be proved by a straightforward calculation, see, e.g., Schneck [14]. $\qquad\square$

Lemma 3.4 *Let f be in $H_0^\alpha(\Omega)$ for $\alpha \geq 1$. Then,*

$$
\big\| (\mathbf{R}^* - \mathbf{R}^*_{h_\vartheta})(\Lambda \otimes I) \mathbf{R} f \big\|_{L^2(\Omega)} \lesssim h_\vartheta^\alpha \, \|f\|_\alpha.
$$

Proof For the time being assume $f \in \mathcal{C}_0^\infty(\Omega)$. We will use a duality argument by Natterer [9]. For $g \in \mathcal{C}_0^\infty(\Omega)$ let

$$
u(\vartheta) := \int_\Omega g(x)\Psi(x^t\omega(\vartheta), \vartheta)\, \mathrm{d}x = \int_{-1}^1 \mathbf{R}g(s, \vartheta)\, \Psi(s, \vartheta)\, \mathrm{d}s
\tag{3.3}
$$

where $\Psi = (\Lambda \otimes I)\mathbf{R} f$. The latter equality follows from the coordinate transformation $x = s\omega(\vartheta) + t\omega^\perp(\vartheta) \mapsto (s, t)$. By a straightforward calculation we find the useful relation

$$
|\langle (\mathbf{R}^* - \mathbf{R}^*_{h_\vartheta})\Psi, g \rangle_{L^2}| = \left| \int_0^{2\pi} u(\vartheta)\, \mathrm{d}\vartheta - h_\vartheta \sum_{j=0}^{2p-1} u(jh_\vartheta) \right| .
$$

Further,

$$\left\|(\mathbf{R}^* - \mathbf{R}_{h_\vartheta}^*)(\Lambda \otimes I)\mathbf{R}f\right\|_{L^2(\Omega)} = \sup_{g \in \mathcal{C}_0^\infty(\Omega)} \frac{|\langle(\mathbf{R}^* - \mathbf{R}_{h_\vartheta}^*)\Psi, g\rangle_{L^2}|}{\|g\|_{L^2}}$$

$$= \sup_{g \in \mathcal{C}_0^\infty(\Omega)} \frac{\left|\int_0^{2\pi} u(\vartheta)\,d\vartheta - h_\vartheta \sum_{j=0}^{2p-1} u(jh_\vartheta)\right|}{\|g\|_{L^2}}.$$

If we are able to bound

$$\int_0^{2\pi} |u^{(2k+1)}(\vartheta)|d\vartheta \lesssim \|f\|_{2k+1}\|g\|_{L^2}, \quad k \in \mathbb{N}_0, \tag{3.4}$$

we have proved Lemma 3.4 via Lemma 3.3 as well as density and interpolation arguments.

Since

$$\int_0^{2\pi} |u^{(m)}(\vartheta)|d\vartheta \leq \int_0^{2\pi}\int_{-1}^1 \left|D_\vartheta^m\left(\mathbf{R}g(s,\vartheta)\,\Psi(s,\vartheta)\right)\right|\,ds\,d\vartheta$$

$$\leq \sum_{j=0}^m \binom{m}{j} \int_0^{2\pi}\int_{-1}^1 \left|(I \otimes D^{m-j})\mathbf{R}g(s,\vartheta)\,(\Lambda \otimes D^j)\mathbf{R}f(s,\vartheta)\right|\,ds\,d\vartheta$$

$$\leq \sum_{j=0}^m \binom{m}{j} \|(I \otimes D^{m-j})\mathbf{R}g\|_{H^{(1/2,j-m)}}\,\|(\Lambda \otimes D^j)\mathbf{R}f\|_{H^{(-1/2,m-j)}}$$

$$\lesssim \sum_{j=0}^m \binom{m}{j} \|\mathbf{R}g\|_{H^{(1/2,0)}}\,\|\mathbf{R}f\|_{H^{(1/2,m)}}$$

$$\overset{(2.9)}{\lesssim} 2^m \|g\|_{L^2}\|f\|_m$$

estimate (3.4) as well as Lemma 3.4 hold true. $\qquad\square$

Now we handle the second error term.

Lemma 3.5 *Let f be in $H_0^\alpha(\Omega)$. Under the assumptions of Theorem 3.1 we have*

$$\left\|(\mathbf{R}^* - \mathbf{R}_{h_\vartheta}^*)\left((I_h\Lambda E_h - \Lambda) \otimes I\right)\mathbf{R}f\right\|_{L^2(\Omega)} \lesssim h_\vartheta h^{\min\{\alpha_{\max}, \alpha-1\}}\|f\|_\alpha.$$

Proof We proceed as in the proof of Lemma 3.4. Again we benefit from duality, density and interpolation. Let f and g be in $\mathcal{C}_0^\infty(\Omega)$. Define u as in (3.3), however, with

$$\Psi = \left((I_h\Lambda E_h - \Lambda) \otimes I\right)\mathbf{R}f.$$

As in the proof of Lemma 3.4 we find that

$$
\begin{aligned}
\int_0^{2\pi} |u'(\vartheta)|\mathrm{d}\vartheta &\leq \|(I \otimes D)\mathbf{R}g\|_{H^{(1/2,-1)}} \|\Psi\|_{H^{(-1/2,1)}} \\
&\quad + \|\mathbf{R}g\|_{H^{(1/2,0)}} \|(I \otimes D)\Psi\|_{H^{(-1/2,0)}} \\
&\leq 2\,\|\mathbf{R}g\|_{H^{(1/2,0)}} \|\Psi\|_{H^{(-1/2,1)}} \\
&\lesssim \|g\|_{L^2} \|\Psi\|_{H^{(-1/2,1)}}.
\end{aligned}
$$

Further,

$$
\begin{aligned}
\|\Psi\|_{H^{(-1/2,1)}} &\leq \|((I_h\Lambda E_h - \Lambda E_h) \otimes I)\,\mathbf{R}f\|_{H^{(-1/2,1)}} \\
&\quad + \|((\Lambda E_h - \Lambda) \otimes I)\,\mathbf{R}f\|_{H^{(-1/2,1)}} \\
&\overset{(2.7)}{\lesssim} h^{\min\{\alpha_I,\alpha-1\}} \|(\Lambda E_h \otimes I)\mathbf{R}f\|_{H^{(\alpha-3/2,1)}} \\
&\quad + \|((E_h - I) \otimes I)\,\mathbf{R}f\|_{H^{(1/2,1)}} \\
&\overset{(2.6)}{\lesssim} h^{\min\{\alpha_I,\alpha-1\}} \|(E_h \otimes I)\mathbf{R}f\|_{H^{(\alpha-1/2,1)}} \\
&\quad + h^{\min\{\beta_{\max},\alpha-1/2\}-1/2} \|\mathbf{R}f\|_{H^{(\alpha-1/2,1)}} \\
&\overset{(2.6)}{\lesssim} \left(h^{\min\{\alpha_I,\tau_{\max}-1/2,\alpha-1\}} + h^{\min\{\beta_{\max}-1/2,\alpha-1\}} \right) \|\mathbf{R}f\|_{H^{(\alpha-1/2,1)}} \\
&\overset{(2.9)}{\lesssim} h^{\min\{\alpha_{\max},\alpha-1\}} \|f\|_\alpha.
\end{aligned}
$$

Thus,

$$
\int_0^{2\pi} |u'(\vartheta)|\mathrm{d}\vartheta \lesssim h^{\min\{\alpha_{\max},\alpha-1\}} \|g\|_{L^2} \|f\|_\alpha.
$$

Finally,

$$
\begin{aligned}
\left\| (\mathbf{R}^* - \mathbf{R}_{h_\vartheta}^*)\Psi \right\|_{L^2(\Omega)} &= \sup_{g \in \mathcal{C}_0^\infty(\Omega)} \frac{\left| \int_0^{2\pi} u(\vartheta)\,\mathrm{d}\vartheta - h_\vartheta \sum_{j=0}^{2p-1} u(jh_\vartheta) \right|}{\|g\|_{L^2}} \\
&\lesssim h_\vartheta \sup_{g \in \mathcal{C}_0^\infty(\Omega)} \frac{\int_0^{2\pi} |u'(\vartheta)|\mathrm{d}\vartheta}{\|g\|_{L^2}} \lesssim h_\vartheta h^{\min\{\alpha_{\max},\alpha-1\}} \|f\|_\alpha
\end{aligned}
$$

ends the proof of Lemma 3.5.   □

Now Theorem 3.1 is established by (3.1), Theorem 2.1, (3.2), Lemmas 3.4 and 3.5.

Remark 3.6 Unfortunately, our convergence analysis of the FBA does not apply to density distributions appearing in medical imaging. Image densities in medical imaging can be considered elements in $H_0^\alpha(\Omega)$ with $\alpha < 1/2$ but close to $1/2$, see Natterer [11, pp. 92ff.]. Theorem 3.1, however, requires $\alpha \geq \alpha_{\min} \geq 1$. The main reason causing this lower bound on the Sobolev regularity is the error estimate for the composite

trapezoidal rule (Lemma 3.3). At present we do not know a useful estimate requiring less smoothness of the integrand.

4 MFBA: a modified filtered backprojection algorithm

In the representation (2.2) of the FBA we see that the Λ-operator is *not* discretized. Rather, it is applied to the continuous function $(E_h \otimes I)\mathbf{R}f(\cdot, \vartheta_j)$ which interpolates or approximates the discrete Radon data with respect to the lateral variable. We suggest an analogous approach to the angular variable, that is, we interpolate the discrete data with respect to both variables. Now, the Λ-operator and the backprojection operator can act exactly on the resulting continuous bivariate function. We call the resulting numerical scheme *modified filtered backprojection algorithm* (MFBA):

$$
\begin{aligned}
f_{\mathrm{MFBA}}(x) :&= \frac{1}{4\pi} \mathbf{R}^*(I_h \otimes I)(\Lambda \otimes I)(E_h \otimes T_{h_\vartheta})\mathbf{R}f(x) \\
&= \frac{1}{4\pi} \mathbf{R}^*(I_h \Lambda E_h \otimes T_{h_\vartheta})\mathbf{R}f(x)
\end{aligned}
\tag{4.1}
$$

with the periodic linear interpolation

$$
T_{h_\vartheta} w(\cdot) = \sum_{j=0}^{2p-1} w(\vartheta_j) C_{h_\vartheta}(\cdot - \vartheta_j)
$$

where C_{h_ϑ} is a 2π-*periodized* linear B-spline. More precisely: Let C be the linear B-spline. Then, $C_{h_\vartheta}(\cdot) = \sum_{k \in \mathbb{Z}} C(\cdot/h_\vartheta + 2\pi k/h_\vartheta)$.

Remark 4.1 In defining T_{h_ϑ} we could in principle replace C by higher order (quadratic, cubic etc.) B-splines. Unfortunately, this would *not* improve the maximal convergence order in (4.2) below, which, in turn, would *not* increase the maximal angular convergence rate α_T in Theorem 4.2 below (compare Theorem A.2 in [12]). To benefit from higher order B-splines one needs to introduce more sophisticated (quasi-)interpolation schemes for the angular variable.

Before we consider a numerical implementation of MFBA we prove convergence with optimal rates.

4.1 Convergence of MFBA

The key for proving convergence of MFBA is the approximation property

$$
\|T_{h_\vartheta} - I\|_{H_p^\alpha(0,2\pi) \to H_p^{-\nu}(0,2\pi)} \lesssim h_\vartheta^{\alpha+\nu}, \qquad 1/2 + \nu < \alpha \leq 2,
\tag{4.2}
$$

for any $0 \leq \nu < 1/2$. We will validate (4.2) below in Theorem 4.3.

Theorem 4.2 *Assume* (2.6) *and* (2.7) *with* $\beta_{\max}, \tau_{\max} \geq 1/2$ *and* $\beta_{\min} < 1$. *Further, let*

$$I_h : L^2(\mathbb{R}) \to L^2(\mathbb{R}) \quad \text{be bounded.} \tag{4.3}$$

Then,

$$\left\| f - \frac{1}{4\pi} \mathbf{R}^*(I_h \Lambda E_h \otimes T_{h_\vartheta}) \mathbf{R} f \right\|_{L^2(\Omega)} \lesssim \left(h^{\min\{\alpha, \alpha_{\max}\}} + h_\vartheta^{\min\{\alpha, \alpha_{\mathrm{T}}\}} \right) \| f \|_\alpha$$

for $\alpha > \alpha_{\min} = 1/2 + 2 \max\{0, \beta_{\min} - 1/2\}$ *where* $\alpha_{\max} = \min\{\alpha_{\mathrm{I}}, \beta_{\max} - 1/2, \tau_{\max} - 1/2\}$ *and any* $\alpha_{\mathrm{T}} < 5/2$.

Proof We will need that

$$I_h : H^{-1/2+\nu}(\mathbb{R}) \to H^{-1/2+\nu}(\mathbb{R}) \quad \text{is a bounded operator} \tag{4.4}$$

which follows from (2.7) and (4.3) via interpolation.

We start with

$$\left\| f - \frac{1}{4\pi} \mathbf{R}^*(I_h \Lambda E_h \otimes T_{h_\vartheta}) \mathbf{R} f \right\|_{L^2}$$

$$\leq \left\| f - \frac{1}{4\pi} \mathbf{R}^*(I_h \Lambda E_h \otimes I) \mathbf{R} f \right\|_{L^2} + \left\| \mathbf{R}^* \left(I_h \Lambda E_h \otimes (T_{h_\vartheta} - I) \right) \mathbf{R} f \right\|_{L^2}$$

$$\lesssim h^{\min\{\alpha, \alpha_{\max}\}} \| f \|_\alpha + \left\| \mathbf{R}^* \left(I_h \Lambda E_h \otimes (T_{h_\vartheta} - I) \right) \mathbf{R} f \right\|_{L^2},$$

the last estimate being due to Theorem 2.1. Bounding the remaining error term is basically straightforward. Under $\max\{0, \beta_{\min} - 1/2\} \leq \nu < 1/2$ we find that

$$\left\| \mathbf{R}^* \left(I_h \Lambda E_h \otimes (T_{h_\vartheta} - I) \right) \mathbf{R} f \right\|_{L^2} \overset{(2.9)}{\lesssim} \left\| \left(I_h \Lambda E_h \otimes (T_{h_\vartheta} - I) \right) \mathbf{R} f \right\|_{H^{(-1/2+\nu, -\nu)}}$$

$$\overset{(4.4)}{\lesssim} \left\| \left(\Lambda E_h \otimes (T_{h_\vartheta} - I) \right) \mathbf{R} f \right\|_{H^{(-1/2+\nu, -\nu)}}$$

$$\lesssim \left\| \left(E_h \otimes (T_{h_\vartheta} - I) \right) \mathbf{R} f \right\|_{H^{(1/2+\nu, -\nu)}}$$

$$\overset{(2.6)}{\lesssim} \left\| \left(I \otimes (T_{h_\vartheta} - I) \right) \mathbf{R} f \right\|_{H^{(1/2+\nu, -\nu)}}$$

$$\overset{(4.2)}{\lesssim} h_\vartheta^\alpha \| \mathbf{R} f \|_{H^{(1/2+\nu, \alpha-\nu)}} \overset{(2.9)}{\lesssim} h_\vartheta^\alpha \| f \|_\alpha$$

where both latter estimates require that $1/2 + 2\nu < \alpha \leq 2 + \nu$. Now we have the freedom to choose ν in the admissible range. Choosing $\nu = \alpha_{\mathrm{T}} - 2$ yields $1/2 + 2(\alpha_{\mathrm{T}} - 2) < \alpha \leq \alpha_{\mathrm{T}}$. On the other hand, by $\nu = \max\{0, \beta_{\min} - 1/2\}$ we obtain $1/2 + 2\max\{0, \beta_{\min} - 1/2\} < \alpha \leq 2 + \max\{0, \beta_{\min} - 1/2\}$. Hence,

$$\left\| \mathbf{R}^* \left(I_h \Lambda E_h \otimes (T_{h_\vartheta} - I) \right) \mathbf{R} f \right\|_{L^2} \lesssim h_\vartheta^\alpha \| f \|_\alpha$$

for $1/2 + 2\max\{0, \beta_{\min} - 1/2\} < \alpha \leq \alpha_{\mathrm{T}} < 5/2$. $\qquad\square$

As a consequence of the above theorem the error estimate (1.4) holds true since the corresponding operators I_h satisfy (4.3), see [12] or [14] for more details.

We complete the present section by finally verifying the approximation property (4.2). The remainder of this subsection is rather technical.

Theorem 4.3 *For any $0 \le \nu < 1/2$ we have that*

$$\|u - T_{h\vartheta} u\|_{H_p^{-\nu}(0, 2\pi)} \lesssim h_\vartheta^{\alpha + \nu} \|u\|_{H_p^\alpha(0, 2\pi)}, \qquad 1/2 + \nu < \alpha \le 2. \tag{4.5}$$

Proof We first show the estimate for $\alpha \in [1, 2]$. Let $\varphi_1 \in \mathcal{C}_0^\infty(0, 2\pi)$ and $\varphi_2 \in \mathcal{C}_p^\infty(0, 2\pi)$ with $\tau_\pi \varphi_2 = \varphi_2(\cdot - \pi) \in \mathcal{C}_0^\infty(0, 2\pi)$ such that $\varphi_1 + \varphi_2 = 1 \in \mathcal{C}_p^\infty(0, 2\pi)$ (partition of unity).[7] Then,

$$\begin{aligned}
\|u - T_{h\vartheta} u\|_{H_p^{-\nu}(0, 2\pi)} &= \|(I - T_{h\vartheta})(\varphi_1 u + \varphi_2 u)\|_{H_p^{-\nu}(0, 2\pi)} \\
&\le \|(I - T_{h\vartheta})(\varphi_1 u)\|_{H_p^{-\nu}(0, 2\pi)} \\
&\quad + \|(I - T_{h\vartheta})(\varphi_2 u)\|_{H_p^{-\nu}(0, 2\pi)} \\
&\lesssim \|(I - T_{h\vartheta})(\varphi_1 u)\|_{H_0^{-\nu}(0, 2\pi)} \\
&\quad + \|((I - T_{h\vartheta})(\varphi_2 u))^*|_{(\pi, 3\pi)}\|_{H_0^{-\nu}(\pi, 3\pi)},
\end{aligned}$$

where w^* denotes the 2π-periodic extension to $\mathbb{R}$ of $w \in H_p^\beta(0, 2\pi), \beta \in \mathbb{R}$. Suppose we are able to show that

$$\|u - T_{h\vartheta} u\|_{H_0^{-\nu}(0, 2\pi)} \lesssim h_\vartheta^{\alpha + \nu} \|u\|_{H_0^\alpha(0, 2\pi)}, \quad 1 \le \alpha \le 2, \tag{4.6}$$

then

$$\begin{aligned}
\|u - T_{h\vartheta} u\|_{H_p^{-\nu}(0, 2\pi)} &\lesssim h_\vartheta^{\alpha + \nu} \left(\|\varphi_1 u\|_{H_0^\alpha(0, 2\pi)} + \|(\varphi_2 u)^*|_{(\pi, 3\pi)}\|_{H_0^\alpha(\pi, 3\pi)} \right) \\
&= h_\vartheta^{\alpha + \nu} \left(\|\varphi_1 u\|_{H_0^\alpha(0, 2\pi)} + \|\tau_\pi (\varphi_2 u)\|_{H_0^\alpha(0, 2\pi)} \right) \\
&\lesssim h_\vartheta^{\alpha + \nu} \|u\|_{H_p^\alpha(0, 2\pi)}, \quad 1 \le \alpha \le 2.
\end{aligned}$$

On the other hand, from [12, Theorem A.2] we know that

$$\|u - T_{h\vartheta} u\|_{L^2(0, 2\pi)} \lesssim h_\vartheta^\alpha \|u\|_{H_p^\alpha(0, 2\pi)}, \quad 1/2 < \alpha \le 2.$$

Hence, we are able to deduce (4.5) by an interpolation argument.

Accordingly, we only need to validate (4.6) to establish Theorem 4.3. We begin with the simple triangle inequality

$$\|v - T_{h\vartheta} v\|_{H_0^{-\nu}(0, 2\pi)} \le \|v - \widetilde{T}_{h\vartheta} v\|_{H_0^{-\nu}(0, 2\pi)} + \|\widetilde{T}_{h\vartheta} v - T_{h\vartheta} v\|_{H_0^{-\nu}(0, 2\pi)} \tag{4.7}$$

---

[7] Note that $|||w||| = \|\varphi_1 w\|_{H_0^\alpha(0, 2\pi)} + \|\tau_\pi (\varphi_2 w)\|_{H_0^\alpha(0, 2\pi)}$ yields a norm on $H_p^\alpha(0, 2\pi)$ being equivalent to the standard norm defined via Fourier coefficients, see, e.g., Lions and Magenes [7, Chap. 1.7].

where $\widetilde{T}_{h_\vartheta}$ is the following auxiliary approximation operator

$$\widetilde{T}_{h_\vartheta} w := h_\vartheta^{-1} \sum_{j=0}^{2p-1} \langle w, C_{h_\vartheta}(\cdot - \vartheta_j)\rangle C_{h_\vartheta}(\cdot - \vartheta_j), \quad w \in L^2(0, 2\pi).$$

For the left summand in (4.7) we find that

$$
\begin{aligned}
\|v - \widetilde{T}_{h_\vartheta} v\|_{H_0^{-\nu}(0,2\pi)} &= \sup_{w \in H^\nu(\mathbb{R})} \frac{|\langle v - \widetilde{T}_{h_\vartheta} v, w\rangle|}{\|w\|_\nu} = \sup_{w \in H^\nu(\mathbb{R})} \frac{|\langle v, w - \widetilde{T}_{h_\vartheta} w\rangle|}{\|w\|_\nu} \\
&\le \|v\|_{L^2(0,2\pi)} \sup_{w \in H^\nu(\mathbb{R})} \frac{\|w - \widetilde{T}_{h_\vartheta} w\|_{L^2(\mathbb{R})}}{\|w\|_\nu} \\
&\lesssim h_\vartheta^\nu \|v\|_{L^2(0,2\pi)}
\end{aligned}
\tag{4.8}
$$

where the last bound is due to [12, Theorem A.2]. We proceed with the right summand of (4.7):

$$\|\widetilde{T}_{h_\vartheta} v - T_{h_\vartheta} v\|_{H_0^{-\nu}(0,2\pi)} = \sup_{w \in H^\nu(\mathbb{R})} \frac{|\langle \widetilde{T}_{h_\vartheta} v - T_{h_\vartheta} v, w\rangle|}{\|w\|_\nu}. \tag{4.9}$$

Since $\widetilde{T}_{h_\vartheta} v - T_{h_\vartheta} v = h_\vartheta^{-1} \sum_{j=0}^{2p-1} \langle v - v(\vartheta_j), C_{h_\vartheta}(\cdot - \vartheta_j)\rangle C_{h_\vartheta}(\cdot - \vartheta_j)$ we have

$$|\langle \widetilde{T}_{h_\vartheta} v - T_{h_\vartheta} v, w\rangle| \le \sum_{j=0}^{2p-1} \underbrace{|\langle v - v(\vartheta_j), h_\vartheta^{-1} C_{h_\vartheta}(\cdot - \vartheta_j)\rangle|}_{=: L_j(v)} |\langle C_{h_\vartheta}(\cdot - \vartheta_j), w\rangle|.$$

We next study the linear functional L_j. For $v \in H^1(\vartheta_{j-1}, \vartheta_{j+1})$ we bound

$$|L_j(v)| \le \int_{\vartheta_{j-1}}^{\vartheta_{j+1}} |v(\vartheta) - v(\vartheta_j)| \, h_\vartheta^{-1} C_{h_\vartheta}(\vartheta - \vartheta_j) \, d\vartheta \le 2\|v\|_{L^\infty(\vartheta_{j-1}, \vartheta_{j+1})}.$$

Further, $L_j(P) = 0$ for any constant P and there is a constant $P = P(v)$ such that the Bramble–Hilbert like estimate

$$\|v - P\|_{L^\infty(\vartheta_{j-1}, \vartheta_{j+1})} \lesssim h_\vartheta^{1/2} \|v\|_{H^1(\vartheta_{j-1}, \vartheta_{j+1})}$$

holds true, see, e.g., Brenner and Scott [2, Proposition 4.3.2]. Combining our findings we have

$$|L_j(v)| = |L_j(v - P)| \lesssim \|v - P\|_{L^\infty(\vartheta_{j-1}, \vartheta_{j+1})} \lesssim h_\vartheta^{1/2} \|v\|_{H^1(\vartheta_{j-1}, \vartheta_{j+1})},$$

so that, for $v \in H_0^1(0, 2\pi)$,

$$
\begin{aligned}
&|\langle \widetilde{T}_{h_\vartheta} v - T_{h_\vartheta} v, w \rangle| \\
&\lesssim h_\vartheta^{1/2} \sum_{j=0}^{2p-1} \|v\|_{H^1(\vartheta_{j-1}, \vartheta_{j+1})} \underbrace{\|C_{h_\vartheta}(\cdot - \vartheta_j)|_{[\vartheta_{j-1}, \vartheta_{j+1}]}\|_{-\nu}}_{\lesssim h_\vartheta^{1/2+\nu} \text{ (Lemma 4.4 below)}} \|w\|_{H^\nu(\vartheta_{j-1}, \vartheta_{j+1})} \\
&\lesssim h_\vartheta^{1+\nu} \left(\sum_{j=0}^{2p-1} \|v\|_{H^1(\vartheta_{j-1}, \vartheta_{j+1})}^2 \right)^{1/2} \left(\sum_{j=0}^{2p-1} \|w\|_{H^\nu(\vartheta_{j-1}, \vartheta_{j+1})}^2 \right)^{1/2} \\
&\lesssim h_\vartheta^{1+\nu} \|v\|_1 \|w\|_\nu.
\end{aligned}
$$

The latter estimate together with (4.9) results in

$$
\|\widetilde{T}_{h_\vartheta} v - T_{h_\vartheta} v\|_{H_0^{-\nu}(0, 2\pi)} \lesssim h_\vartheta^{1+\nu} \|v\|_1, \quad v \in H_0^1(0, 2\pi),
$$

which in combination with (4.7) and (4.8) implies that

$$
\|v - T_{h_\vartheta} v\|_{H_0^{-\nu}(0, 2\pi)} \lesssim h_\vartheta^\nu \|v\|_{L^2(0, 2\pi)} + h_\vartheta^{1+\nu} \|v\|_1, \quad v \in H_0^1(0, 2\pi).
$$

For $u \in H_0^\alpha(0, 2\pi)$, $1 \leq \alpha \leq 2$, set $v := u - T_{h_\vartheta} u \in H_0^1(0, 2\pi)$. Note that $v - T_{h_\vartheta} v = u - T_{h_\vartheta} u$. Finally, (4.6) is established by

$$
\begin{aligned}
\|u - T_{h_\vartheta} u\|_{H_0^{-\nu}(0, 2\pi)} &= \|v - T_{h_\vartheta} v\|_{H_0^{-\nu}(0, 2\pi)} \lesssim h_\vartheta^\nu \|v\|_{L^2(0, 2\pi)} + h_\vartheta^{1+\nu} \|v\|_1 \\
&= h_\vartheta^\nu \|u - T_{h_\vartheta} u\|_{L^2(0, 2\pi)} + h_\vartheta^{1+\nu} \|u - T_{h_\vartheta} u\|_1 \\
&\lesssim h_\vartheta^{\alpha+\nu} \|u\|_\alpha
\end{aligned}
$$

where in the last step we once more applied Theorem A.2 of [12]. Thus, Theorem 4.3 is completely verified. $\qquad\square$

Lemma 4.4 *To any $0 \leq \nu < 1/2$ there is a constant $c = c(\nu)$ such that*

$$
\|C_{h_\vartheta}|_{[-h_\vartheta, h_\vartheta]}\|_{-\nu} \leq c(\nu) h_\vartheta^{1/2+\nu}.
$$

Proof We have

$$
\begin{aligned}
&\|C_{2h_\vartheta}|_{[-2h_\vartheta, 2h_\vartheta]}\|_{-\nu}^2 \\
&= \int_{\mathbb{R}} (1 + |\sigma|^2)^{-\nu} |\widehat{C_{2h_\vartheta}}(\sigma)|^2 \, d\sigma = 4h_\vartheta^2 \int_{\mathbb{R}} (1 + |\sigma|^2)^{-\nu} |\widehat{C}(2h_\vartheta \sigma)|^2 \, d\sigma
\end{aligned}
$$

$$= 4\sqrt{2\pi}h_\vartheta^2 \int_{\mathbb{R}} (1 + |\sigma|^2)^{-\nu} |\mathrm{sinc}^2(h_\vartheta\sigma)|^2 \, d\sigma$$

$$= 4\sqrt{2\pi}h_\vartheta^2 \left(\int_{-h_\vartheta^{-1}}^{h_\vartheta^{-1}} (1 + |\sigma|^2)^{-\nu} \underbrace{|\mathrm{sinc}^2(h_\vartheta\sigma)|^2}_{\leq 1} \, d\sigma \right.$$

$$\left. + \int_{\mathbb{R}\setminus[-h_\vartheta^{-1},h_\vartheta^{-1}]} (1 + |\sigma|^2)^{-\nu} \underbrace{|\mathrm{sinc}^2(h_\vartheta\sigma)|^2}_{\leq (h_\vartheta\sigma)^{-4}} \, d\sigma \right)$$

$$\leq 4\sqrt{2\pi}h_\vartheta^2 \left(\underbrace{\int_{-h_\vartheta^{-1}}^{h_\vartheta^{-1}} |\sigma|^{-2\nu} \, d\sigma}_{= \frac{2}{1-2\nu}h_\vartheta^{2\nu-1}} + h_\vartheta^{-4} \underbrace{\int_{\mathbb{R}\setminus[-h_\vartheta^{-1},h_\vartheta^{-1}]} |\sigma|^{-2\nu-4} \, d\sigma}_{= \frac{2}{2\nu+3}h_\vartheta^{2\nu+3}} \right)$$

$$= 8\sqrt{2\pi} \left(\frac{1}{1-2\nu} + \frac{1}{2\nu+3} \right) h_\vartheta^{1+2\nu}.$$

Thus, $c(\nu) = 2^{2-\nu}\sqrt{\sqrt{2\pi}\left(\frac{1}{1-2\nu} + \frac{1}{2\nu+3} \right)}$.   □

4.2 Implementation of MFBA

We discuss some aspects concerning the numerical evaluation of $f_{\mathrm{MFBA}}(x)$, see (4.1).
Define $\Phi := \frac{1}{4\pi}(I_h \Lambda E_h \otimes I)\mathbf{R}f$. Then,

$$\Phi(s, \vartheta) = \sum_{k \in \mathbb{Z}} g_k(\vartheta) A_h(s - s_k)$$

where

$$g_k(\vartheta) = \frac{1}{4\pi}h^{-1}\langle (\Lambda E_h \otimes I)\mathbf{R}f(\cdot, \vartheta), \eta_h(\cdot - s_k)\rangle$$

are the filtered Radon data, compare (2.5). We obtain

$$f_{\mathrm{MFBA}}(x) = \frac{1}{4\pi}\mathbf{R}^*(I_h \Lambda E_h \otimes T_{h_\vartheta})\mathbf{R}f(x) = \int_0^{2\pi} (I \otimes T_{h_\vartheta})\Phi(x^t\omega(\vartheta), \vartheta) \, d\vartheta$$

$$= \int_0^{2\pi} \sum_{j=0}^{2p-1} \Phi(x^t\omega(\vartheta), \vartheta_j)C_{h_\vartheta}(\vartheta - \vartheta_j) \, d\vartheta$$

$$= \int_0^{2\pi} \sum_{j=0}^{2p-1} \sum_{k\in\mathbb{Z}} g_k(\vartheta_j) A_h(x^t \omega(\vartheta) - s_k) C_{h_\vartheta}(\vartheta - \vartheta_j) \, d\vartheta$$

$$= \sum_{k\in\mathbb{Z}} \sum_{j=0}^{2p-1} g_k(\vartheta_j) \int_0^{2\pi} A_h(x^t \omega(\vartheta) - s_k) C_{h_\vartheta}(\vartheta - \vartheta_j) \, d\vartheta.$$

Observe that $f_{\mathrm{MFBA}}(0) = f_{\mathrm{FBA}}(0)$.

To reduce the notational burden we introduce the abbreviation

$$I(s, \psi, x) = \int_0^{2\pi} A_h(x^t \omega(\vartheta) - s) C_{h_\vartheta}(\vartheta - \psi) \, d\vartheta.$$

Since $g_k(\vartheta_j) = g_{-k}(\vartheta_{j+p})$ as well as $I(s_k, \vartheta_j, x) = I(s_{-k}, \vartheta_{j+p}, x)$ we have that

$$f_{\mathrm{MFBA}}(x) = 2 \sum_{k\in\mathbb{Z}} \sum_{j=0}^{p-1} g_k(\vartheta_j) I(s_k, \vartheta_j, x).$$

It remains to compute the integrals $I(s_k, \vartheta_j, x)$. A straightforward calculation gives that $(x \neq 0)$

$$I(s_k, \vartheta_j, x) = I(s_k, \vartheta_j - \arg(x), |x|\omega(0)).^{[8]}$$

Thus, we only need to evaluate integrals like

$$I(s_k, \psi, r\omega(0)) = \int_{\psi - h_\vartheta}^{\psi + h_\vartheta} A_h(r\cos(\vartheta) - s_k) C_{h_\vartheta}(\vartheta - \psi) \, d\vartheta.$$

For $A = \mathbf{1}_{[-1/2,1/2]}$ and $A = \mathbf{1}_{[-1/2,1/2]} \star \mathbf{1}_{[-1/2,1/2]}$ an explicit computation of the above integrals can be found in [14]. Please note that most of the integrals are zero and do not need to be computed. For instance, if $A = \mathbf{1}_{[-1/2,1/2]} \star \mathbf{1}_{[-1/2,1/2]}$ then

$$[\min \Theta(\psi, h_\vartheta), \max \Theta(\psi, h_\vartheta)] \cap \left[\frac{s_{k-1}}{r}, \frac{s_{k+1}}{r} \right] = \emptyset \implies I(s_k, \psi, r\omega(0)) = 0$$

where $\Theta(\psi, h_\vartheta) = \cos([\psi - h_\vartheta, \psi + h_\vartheta])$.

Remark 4.5 In principle, the band matrix $M(x) = \{I(s_k, \vartheta_j, x)\}_{k,j}$ can be precomputed and stored as its entries only depend on the scanning geometry and the reconstruction points where $M(-x)_{k,j} = M(x)_{-k,j}$. Moreover, the bandwidth of M depends only on the ratio h_ϑ / h.

---

[8] $\arg(x)$ denotes the angle in the polar representation of $x \in \mathbb{R}^2 \setminus \{0\}$: $x = |x|\omega(\arg(x))$.

Therefore, if $h = h_\vartheta$ and if the sparse matrices M are precomputed, FBA and MFBA require essentially the same number of arithmetic operations. The ratio of the complexities of MFBA and FBA increases linearly with h_ϑ / h.

In our numerical experiments in the following section we however, computed the non-zero entries of M on-the-fly.

4.3 MFBA is the limit of the phantom view algorithm

Weiss et al. [17] have analyzed an FBA-based algorithm to reduce streak artifacts in CT reconstructions caused by angular under-sampling (see, e.g., Galigekere et al. [3] for further work in this direction). They considered so-called "phantom views" by interpolating the Radon data linearly with respect to the angular variable. We call this algorithm PhanFBA(R) where $R - 1$ is the number of interpolated (phantom) views between measured views. PhanFBA(2) has first been suggested by Lewitt et al. [6, Sect. 5.3].

Starting out from the discrete Radon data D (1.1) we have that

$$f_{\text{PhanFBA}(R)}(x) = \underbrace{\frac{1}{4\pi} \mathbf{R}^*_{h_\vartheta / R}(I_h \Lambda E_h \otimes I)}_{\text{Step 2}} \underbrace{(I \otimes T_{h_\vartheta})}_{\text{Step 1}} \mathbf{R} f(x)$$

$$= \frac{1}{4\pi} \mathbf{R}^*_{h_R}(I_h \Lambda E_h \otimes T_{h_\vartheta}) \mathbf{R} f(x)$$

where first the Radon data are linearly interpolated (Step 1) and then (Step 2) standard FBA is applied with angular discretization step size $h_R = h_\vartheta / R = \pi/(Rp)$, $R \in \mathbb{N}$. Observe that

$$f_{\text{FBA}}(0) = f_{\text{MFBA}}(0) = f_{\text{PhanFBA}(R)}(0). \tag{4.10}$$

We expect convergence of $f_{\text{PhanFBA}(R)}$ to f_{MFBA} for increasing R. In fact,

$$\begin{aligned} &\| f_{\text{MFBA}} - f_{\text{PhanFBA}(R)} \|_{L^2(\Omega)} \\ &\lesssim \frac{1}{R} \left(h_\vartheta h^{\min\{\alpha_{\max}, \alpha - 1\}} + h_\vartheta^{\min\{2, \alpha\}} \right) \| f \|_\alpha, \quad \alpha \ge 1. \end{aligned} \tag{4.11}$$

The latter estimate follows directly from our previous results. We start with

$$\begin{aligned} \| f_{\text{MFBA}} - f_{\text{PhanFBA}(R)} \|_{L^2} &\le \| (\mathbf{R}^* - \mathbf{R}^*_{h_R})(I_h \Lambda E_h \otimes (T_{h_\vartheta} - I)) \mathbf{R} f \|_{L^2} \\ &\quad + \| (\mathbf{R}^* - \mathbf{R}^*_{h_R})(I_h \Lambda E_h \otimes I) \mathbf{R} f \|_{L^2}. \end{aligned}$$

For $\alpha \ge 1$,

$$\| (\mathbf{R}^* - \mathbf{R}^*_{h_R})(I_h \Lambda E_h \otimes I) \mathbf{R} f \|_{L^2} \lesssim \left(h_R^\alpha + h_R h^{\min\{\alpha_{\max}, \alpha - 1\}} \right) \| f \|_\alpha$$

by (3.2), Lemma 3.4, and Lemma 3.5. Copying the proof of Lemma 3.5 we find that

$$\|(\mathbf{R}^* - \mathbf{R}_{h_R}^*)\Psi\|_{L^2} \lesssim h_R \|\Psi\|_{H^{(-1/2,1)}} \text{ with } \Psi := (I_h \Lambda E_h \otimes (T_{h_\vartheta} - I))\mathbf{R}f.$$

Further,

$$\|\Psi\|_{H^{(-1/2,1)}} \overset{(4.4)}{\lesssim} \|(\Lambda E_h \otimes (T_{h_\vartheta} - I))\mathbf{R}f\|_{H^{(-1/2,1)}}$$

$$\overset{(2.6)}{\lesssim} \|(E_h \otimes (T_{h_\vartheta} - I))\mathbf{R}f\|_{H^{(1/2,1)}} \lesssim \|(I \otimes (T_{h_\vartheta} - I))\mathbf{R}f\|_{H^{(1/2,1)}}$$

$$\lesssim h_\vartheta^{\min\{1,\alpha-1\}} \|\mathbf{R}f\|_{H^{(1/2,\alpha)}} \overset{(2.9)}{\lesssim} h_\vartheta^{\min\{1,\alpha-1\}} \|f\|_\alpha$$

where the second to last estimate follows from Theorem A.2 of [12]. Thus, (4.11) is established. Finally, under the assumptions of Theorem 4.2 a triangle inequality yields

$$\|f - f_{\text{PhanFBA}(R)}\|_{L^2(\Omega)} \lesssim \left(h^{\min\{\alpha,\alpha_{\max}\}} + h_\vartheta^{\min\{\alpha,\alpha_T\}} \right.$$

$$\left. + \frac{1}{R} \left(h_\vartheta h^{\min\{\alpha_{\max},\alpha-1\}} + h_\vartheta^{\min\{2,\alpha\}} \right) \right) \|f\|_\alpha, \quad \alpha \geq 1.$$

Under a moderately large number R of phantom views, PhanFBA(R) mimics the asymptotic convergence behavior of MFBA whose convergence order in h_ϑ may exceed the order in h (in case $\alpha_{\max} < \alpha_T$ and $\alpha > \alpha_{\max}$).

Finally, we provide a different interpretation of PhanFBA(R) and MFBA by generalizing an observation by Lewitt et al. [6, Eq. (40)]. Set $\Phi := (I_h \Lambda E_h \otimes T_{h_\vartheta})\mathbf{R}f$ and let $U_\varphi \in \mathbb{R}^{2\times 2}$ be the rotation matrix by angle φ. Taking into account that $x^t\omega(\vartheta_{j+\frac{\ell}{R}}) = (U_{\frac{\ell}{R}h_\vartheta}x)^t\omega(\vartheta_j)$[9] we obtain

$$f_{\text{PhanFBA}(R)}(x)$$

$$= \frac{h_\vartheta}{R} \sum_{j=0}^{2p-1} \sum_{\ell=0}^{R-1} \Phi(x^t\omega(\vartheta_{j+\ell/R}), \vartheta_{j+\ell/R})$$

$$= \frac{h_\vartheta}{R} \sum_{j=0}^{2p-1} \sum_{\ell=0}^{R-1} \left(\left(1 - \frac{\ell}{R}\right) \Phi(x^t\omega(\vartheta_{j+\ell/R}), \vartheta_j) + \frac{\ell}{R} \Phi(x^t\omega(\vartheta_{j+\ell/R}), \vartheta_{j+1}) \right)$$

$$= \frac{1}{R} \left(f_{\text{FBA}}(x) + \sum_{\ell=1}^{R-1} \left(1 - \frac{\ell}{R}\right) \left(f_{\text{FBA}}(U_{\frac{\ell}{R}h_\vartheta}x) + f_{\text{FBA}}(U_{-\frac{\ell}{R}h_\vartheta}x) \right) \right).$$

Letting R approach infinity yields

$$f_{\text{MFBA}}(x) = \frac{1}{h_\vartheta} \int_{-h_\vartheta}^{h_\vartheta} f_{\text{FBA}}(U_\varphi x) \, B_{h_\vartheta}(\varphi) \, d\varphi \tag{4.12}$$

where B is the linear B-spline. Thus, MFBA is an angular average of FBA.

---

[9] $\vartheta_{j+\frac{\ell}{R}} := \left(j + \frac{\ell}{R}\right) h_\vartheta$

5 Numerical illustrations

Numerical experiments illustrating the convergence orders of FBA (Theorem 3.1) under the optimal sampling condition $p = \pi q$ can already be found in [12, Sect. 6]. Further experiments are reported in [14]. We therefore concentrate on experiments highlighting the different convergence behaviors of the algorithms in the lateral and angular variables. Additionally, we compare FBA, MFBA, and PhanFBA(R) qualitatively.

First we demonstrate that the error term of FBA behaving like h_ϑ^α does indeed not saturate, see (1.2). To this end, we reconstruct a function $f \in H_0^{5/2}(\Omega)$ from discrete data D, see (1.1), with $q = \lfloor p^{5/3} \rfloor$ using the Shepp-Logan filter with piecewise constant interpolation ($\alpha_{\max} = 3/2$). From (1.2) we expect the convergence rate $p^{-5/2}$ as $p \to \infty$.

As density distribution f we use

$$f(x) := \sum_{k=1}^{3} d_k \, P\left(U_k(x - b_k)\right) \tag{5.1}$$

where $P(x) = (1 - |x|^2)^{2.01}$, $|x| \leq 1$, and $P(x) = 0$, otherwise, and $d_1 = 1$, $d_2 = -1.5$, $d_3 = 1.5$, and $b_1 = (0.22, 0)^t$, $b_2 = (-0.22, 0)^t$, $b_3 = (0, 0.2)^t$. Further, $U_k = U(\varphi_k, \delta_k, \gamma_k)$, $k = 1, 2, 3$, with

$$U(\varphi, \delta, \gamma) := \begin{pmatrix} \cos(\varphi)/\delta & \sin(\varphi)/\delta \\ -\sin(\varphi)/\gamma & \cos(\varphi)/\gamma \end{pmatrix}$$

and

$\delta_1 = 0.51,$	$\gamma_1 = 0.31,$	$\varphi_1 = 72\pi/180,$
$\delta_2 = 0.51,$	$\gamma_2 = 0.36,$	$\varphi_2 = 108\pi/180,$
$\delta_3 = 0.5,$	$\gamma_3 = 0.8,$	$\varphi_3 = \pi/2.$

Note that $f \in H_0^\alpha(\Omega)$ for any $\alpha < 2.51$. For a graphical representation of f see [12, Fig. 2]. The Radon transform of f can be computed analytically. From discrete Radon data we reconstructed

$$f_{\text{FBA},q,p}(x) = \frac{1}{4\pi} \mathbf{R}_{\pi/p}^* (I_{1/q} \Lambda E_{1/q} \otimes I) \mathbf{R} f(x), \quad x \in \mathcal{X},$$

on the grid $\mathcal{X} := \Omega \cap \{(i/100, j/100) : -100 \leq i, j \leq 100\}$. Now we define the relative L^2-reconstruction error by

$$e(q, p) := \left(\sum_{x \in \mathcal{X}} \left(f_{\text{FBA},q,p}(x) - f(x) \right)^2 \bigg/ \sum_{x \in \mathcal{X}} f(x)^2 \right)^{1/2}. \tag{5.2}$$

Fig. 1 The relative L^2-errors $e\left(\lfloor p^{5/3}\rfloor, p\right)$ (5.2) for reconstructing f (5.1) by FBA using the Shepp-Logan filter with nearest neighbor interpolation. The auxiliary *solid line* indicates exact decay $p^{-5/2}$. Here, the angular under-sampling (relative to the lateral sampling) is $1/(3p^{2/3})$ ranging from 0.11 ($p = 5$) to 0.02 ($p = 70$)
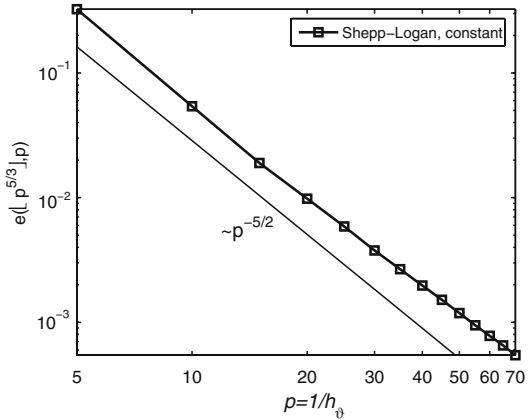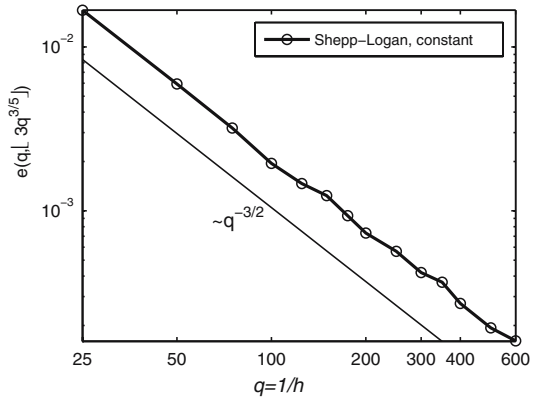

Fig. 2 The relative L^2-errors $e\left(q, \lfloor 3q^{3/5}\rfloor\right)$ (5.2) with f from (5.1) and $f_{FBA,q,p}$ replaced by $f_{MFBA,q,p}$ (Shepp-Logan filter and nearest neighbor interpolation). The auxiliary *solid line* indicates exact decay $q^{-3/2}$. Here, the angular under-sampling (relative to the lateral sampling) is $q^{-2/5}$ ranging from 0.28 ($q = 25$) to 0.08 ($q = 600$)

In Fig. 1 we plotted $e\left(\lfloor p^{5/3}\rfloor, p\right)$ for $p \in \{5l : l = 1, \ldots, 14\}$. Its decay $O(q^{-5/2})$ complies exactly with the prediction by (1.2).

Next we illustrate that the convergence order of MFBA in the angular variable may exceed the order in the lateral variable. Let f from (5.1) be reconstructed by

$$f_{MFBA,q,p}(x) = \frac{1}{4\pi}\mathbf{R}^*(\mathrm{I}_{1/q}\Lambda E_{1/q} \otimes T_{\pi/p})\mathbf{R}f(x), \quad x \in \mathcal{X},$$

with Shepp-Logan filter and nearest neighbor interpolation ($\alpha_{max} = 3/2$) where $p = \lfloor 3q^{3/5}\rfloor$. In view of (1.4) we expect an error decay rate like $q^{-3/2+\epsilon}$ for any $\epsilon > 0$ which we indeed observe in Fig. 2.

Now we compare FBA and MFBA. We computed relative L^2-errors for the reconstruction of different test objects (e.g. the functions from (5.1) and Fig. 3) for increasing q and $p = 3q$. It turned out that FBA and MFBA are practically identical in terms of L^2-errors, see Fig. 5. This observation remains true when artificial noise corrupts the data. As the L^2-norm is known not to comply well with the human perception of images we inspected reconstructions visually: Near to edges and vertices we

Fig. 3 Superposition of indicator functions of two rectangles


Fig. 4 Close-ups of reconstructions of the function from Fig. 3 (Shepp-Logan filter, piecewise linear interpolation, $q = 50$, $p = 150$). *Top* FBA, *bottom* MFBA
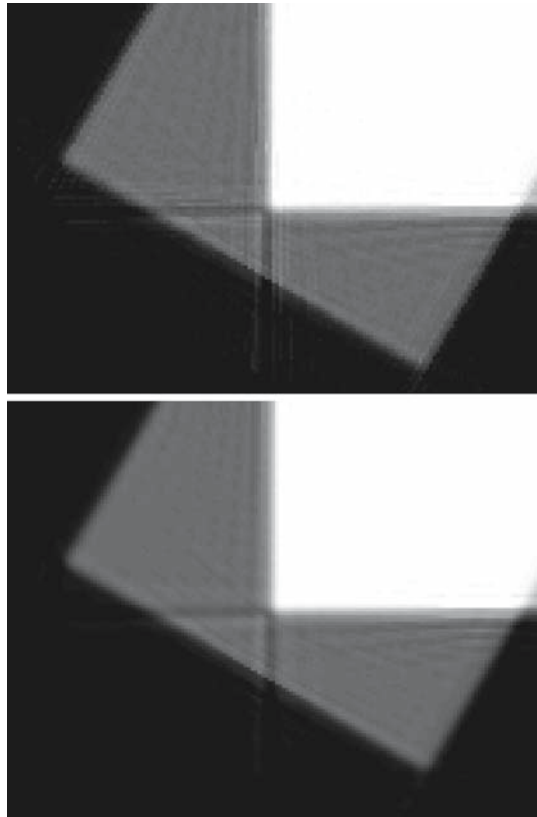
found the artifacts of MFBA less pronounced than those of FBA. For a typical example we reconstruct the function displayed in Fig. 3 being a superposition of indicator functions of two rectangles (For an analytical description see [12, Sect. 6]).

In Fig. 4 we show close-ups of the reconstructions by FBA and MFBA, respectively. Both reconstructions are based on the Shepp-Logan filter with piecewise linear interpolation where $q = 50$ and $p = 150$. MFBA clearly produces less artefacts which are, moreover, less severe. Accordingly the regions of constant gray values appear more homogeneous, however, at the price of blurred edges.

Fig. 5 Quantitative comparison of FBA and MFBA with respect to the BV- and L^2-norm under optimal sampling $p = 3q$. The underlying function is from Fig. 3. *Solid line* with *square* rel. BV-error of MFBA, *solid line* with *circle* rel. L^2-error of MFBA. *Dashed line* with *filledstar* rel. BV-error of FBA, *dashed line* with *triangle* rel. L^2-error of FBA
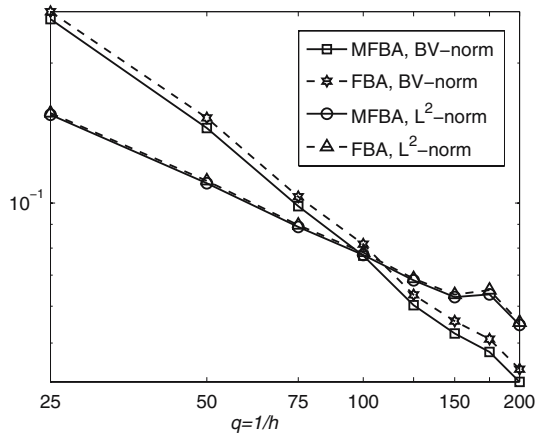
Within the image processing community the norm of bounded variation,

$$\|f\|_{\mathrm{BV}} := \int_\Omega |f(x)|\mathrm{d}x + \int_\Omega |\nabla f|,^{10}$$

is considered a measure for comparing images which is almost as sensitive as the human eye: Both, errors in edges and noise, result in a large BV-norm.

Figure 5 displays the relative BV- and L^2-errors for reconstructing the function of Fig. 3 from discrete data where $q \in \{25, 50, 75, 100, 125, 150, 175, 200\}$ and $p = 3q$. Both algorithms, FBA and MFBA, rely on the Shepp-Logan filter with piecewise linear interpolation. While FBA and MFBA produce virtually identical L^2-errors, the corresponding BV-errors differ slightly. MFBA outperforms FBA with respect to both error measures. Interestingly, the BV-errors decay faster than the L^2-errors, roughly like $O(q^{-3/4})$. So far, we have no analytic explanation for this numerically observed order of decay.

Finally, we demonstrate the streak-diminishing power of PhanFBA(R) and MFBA. Figure 6 displays reconstructions of the Shepp-Logan head phantom [15]. The streak artifacts by FBA due to insufficient angular sampling ($q = 500$, $p = 30$) corrupt the whole reconstruction. MFBA greatly diminishes streaks but causes slightly blurred edges. For instance, the three small ellipses below the two large black ellipses cannot be distinguished anymore. Introducing one phantom view (PhanFBA(2)) already reduces streaks and four phantom views (PhanFBA(5)) yield a reconstruction close to the one by MFBA. The reconstructions by MFBA and PhanFBA(15) (not presented) are virtually identical.

Inspecting Fig. 6 we observe that all four reconstructions match in the vicinity of the origin (middle of the images between the two large black ellipses). This effect was

---

10 The second integral is a symbolic notation for the total variation of f (∇f is a bounded Radon vector measure in general), see, e.g., Giusti [4]. If $f \in W^{1,1}(\Omega)$ then $\int_\Omega |\nabla f| = \int_\Omega |\nabla f(x)|\mathrm{d}x$.
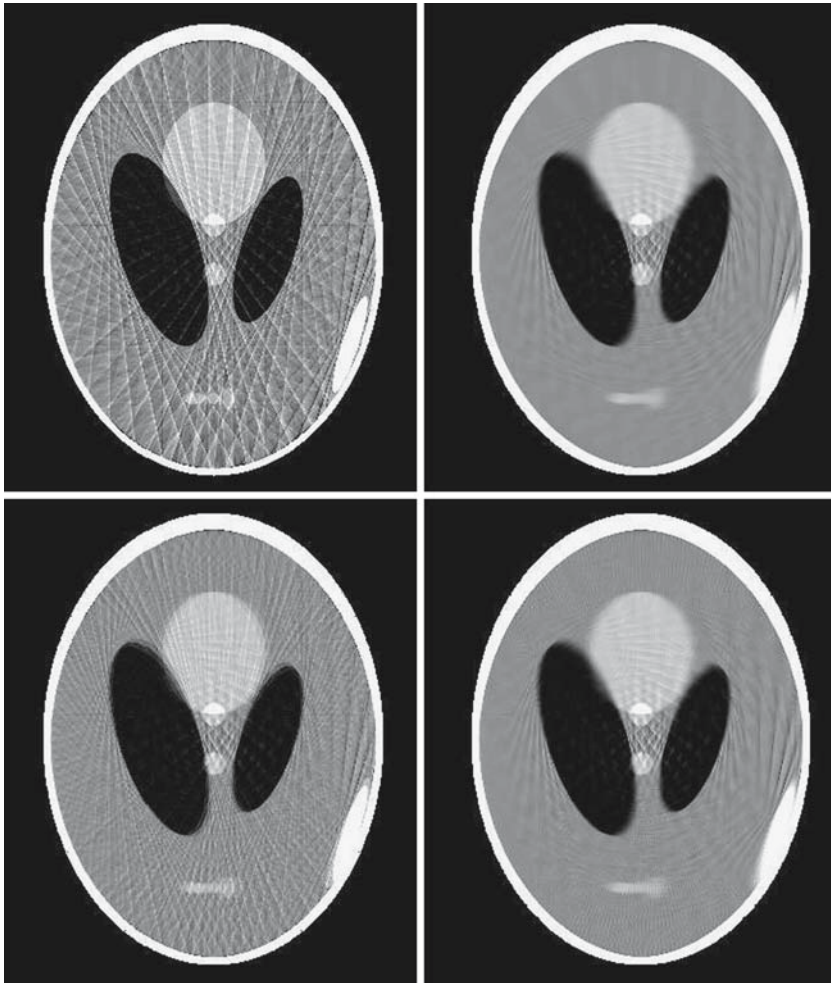
Fig. 6 Reconstructions of Shepp-Logan head phantom [15] (Shepp-Logan filter, piecewise linear interpolation, $q = 500$, $p = 30$). *Top left* FBA, *top right* MFBA. *Bottom left* PhanFBA(2), *bottom right* PhanFBA(5)

already noticed by Weiss et al. [17, Fig. 5] and can analytically be explained by (4.10) as well as by (4.12).

Furthermore, some edges are blurred by MFBA and others are not. The angular average (4.12) provides an explanation: If an edge is tangent to a circle centered about the origin then MFBA does not blur it. The more transversally it intersects such a circle the more it gets blurred. Therefore the parts of streaks being tangent to an origin-centered circle are neither diminished by PhanFBA(R) nor by MFBA.

References

1. Aubin, J.-P.: Applied Functional Analysis, Pure & Applied Mathematics, 2nd edn. Wiley, New York (2000)
2. Brenner, S.C., Scott, L.R.: The Mathematical Theory of Finite Element Methods, vol. 15 of Texts in Applied Mathematics. Springer, New York (1994)
3. Galigekere, R.R., Wiesent, K., Holdsworth, D.W.: Techniques to alleviate the effects of view aliasing artifacts in computed tomography. Med. Phys. **26**, 896–904 (1999)
4. Giusti, E.: Minimal Surfaces and Functions of Bounded Variation. Birkhäuser, Basel (1984)
5. Kress, R.: Numerical Analysis, vol. 181 of Graduate Texts in Mathematics. Springer, New York (1998)
6. Lewitt, R.M., Bates, R.H.T., Peters, T.M.: Image reconstruction from projections II: Modified backprojection methods. Optik **50**, 85–109 (1978)
7. Lions, J.L., Magenes, E.: Non-Homogeneous Boundary Value Problems and Applications, Vol. 1. Springer, New York (1972)
8. Louis, A.K., Natterer, F.: Mathematical problems in computerized tomography. Proc. IEEE **71**, 379–389 (1983)
9. Natterer, F.: Genauigkeitsfragen bei der numerischen Rekonstruktion von Bildern, vol. 49 of International series of numerical mathematics (ISNM), Birkhäuser Verlag, Basel, Switzerland, pp. 131–146 (1979)
10. Natterer, F.: A Sobolev space analysis of picture reconstruction. SIAM J. Appl. Math. **39**, 402–411 (1980)
11. Natterer, F.: The Mathematics of Computerized Tomography. Wiley, Chichester (1986)
12. Rieder, A., Faridani, A.: The semi-discrete filtered backprojection algorithm is optimal for tomographic inversion. SIAM J. Numer. Anal. **41**, 869–892 (2003)
13. Rieder, A., Schuster, Th.: The approximate inverse in action with an application to computerized tomography. SIAM J. Numer. Anal. **37**, 1909–1929 (2000)
14. Schneck, A.: Konvergenz von Rekonstruktionsalgorithmen in der 2D-Tomographie: Der voll-diskrete Fall (Convergence of reconstruction algorithms in 2D-tomography: The fully discrete case). Diploma thesis, Fakultät für Mathematik, Universität Karlsruhe, D-76128 Karlsruhe, Germany (2006)
15. Shepp, L.A., Logan, B.F.: The Fourier reconstruction of a head section. IEEE Trans. Nucl. Sci. **21**, 21–43 (1974)
16. Smithey, D.T., Beck, M., Raymer, M.G., Faridani, A.: Measurement of the Wigner distribution and the density matrix of a light mode using optical homodyne tomography: application to squeezed states and the vacuum. Phys. Rev. Lett. **70**, 1244–1247 (1993)
17. Weiss, G.H., Talbert, A.J., Brooks, R.A.: The use of phantom views to reduce CT streaks due to insufficient sampling. Phys. Med. Biol. **27**, 1151–1162 (1982)